Electromagnetic Waves in Multilayered Generalized Anisotropic Media

Article *in* IEEE Transactions on Geoscience and Remote Sensing · May 2018

DOI: 10.1109/TGRS.2018.2825430

5 authors, including:

Yunyun Hu
Duke University
35 PUBLICATIONS **334** CITATIONS
SEE PROFILE

Yuan Fang
Duke University
30 PUBLICATIONS **489** CITATIONS
SEE PROFILE

Dezhi Wang
Duke University
20 PUBLICATIONS **177** CITATIONS
SEE PROFILE

Qing Huo Liu
Duke University
1,450 PUBLICATIONS **28,314** CITATIONS
SEE PROFILE

Electromagnetic Waves in Multilayered Generalized Anisotropic Media

Yunyun Hu, Yuan Fang, Dezhi Wang, Yu Zhong, and Qing Huo Liu, *Fellow, IEEE*

***Abstract*— This paper presents the formulations for calculating the electromagnetic (EM) fields in multilayered generalized anisotropic media. Maxwell's equations are written into a first-order differential (in z) equation concerning the transverse electric and magnetic field components in the spectral domain. The equation can be solved to obtain the EM fields in a homogeneous anisotropic medium. For fields in layered anisotropic media, the local transmission and reflection matrices, the global reflection matrices, and the recursion relations of the wave amplitudes at interfaces are derived and used to express the EM fields in arbitrary layers. The electric and magnetic dipole sources can locate in arbitrary layers, and the medium can have both full-tensor magnetic and dielectric anisotropy. The singular behavior of the solution in the close vicinity of the dipole source is subtracted to make the integrands decay rapidly as functions of k_x and k_y. The contributions of the subtracted part are calculated analytically. A three-layer anisotropic medium is modeled to show the convergence of the integrals with the singularity subtraction. To validate the algorithm for multilayered generalized anisotropic media, a five-layer medium is modeled and compared with finite element method results. The algorithm is also applied in geophysical EM well logging by modeling the triaxial induction logging tool. The responses in vertical and deviated wells are computed and compared with finite element results. The good agreement between the two results further validates the algorithm and demonstrates its capability to model induction logging tools in multilayered generalized anisotropic media.**

***Index Terms*— Electromagnetic (EM) fields, geophysical electromagnetic well logging, global reflection matrices, layered generalized anisotropic media, local reflection matrices.**

I. Introduction

In the past few decades, considerable attention has been given to electromagnetic (EM) waves in layered structures, concerning various fields including geophysical exploration, microwave remote sensing, wave propagation, microstrip circuits, antennas, and so on [1]–[6]. The EM waves in anisotropic laminates are of much concern and have been studied by many researchers. References [1] and [7]–[12] analyze the problem of dipole antennas over a layered uniaxial medium with the optical axis perpendicular to the plane of stratification, and [13] extends it to arbitrarily oriented optical axes. The problem of a dipole in the presence of planar generalized anisotropic media has been investigated using the propagation matrix method in conjunction with the Fourier transformation technique [14]–[16]. However, this method suffers from numerical instability due to evanescent waves [17], [18]. Recurrence relations (RR) are proposed to cope with the instability [18], [19]. Yang [18] derives the formula for a plane wave incident on a multilayered anisotropic structure with the top and bottom layer interfaces either ground plane or next to a free space. Zhong *et al.* [19] extend the RR to account for an active electric source. Other RR involving impedance and hydrbid matrix methods are introduced in [20] and [21] for EM waves in bianisotropic media.

In this paper, Maxwell's equations in the spectral domain are written into a first-order vector equation concerning the four transverse electric and magnetic field components [15]. The global reflection matrices and recursion relations of wave amplitudes at interfaces [22] are derived and used to express the four-component vector in any regions. The EM fields in the spatial domain are then computed with Fourier transformation. The medium can be multilayered generalized anisotropic with both the dielectric and magnetic anisotropy. The source can be both the magnetic and electric types with arbitrary orientation located in arbitrary layers.

In this paper, we derive the first-order vector equation in Section II-A. In Sections II-B and II-C, the local reflection and transmission matrices, the global reflection matrices, and the recursion relations of wave amplitudes at interfaces are derived and used to express EM fields everywhere. In Section II-C, a three-layer anisotropic case is studied to compare the decaying of the integrands as a function of k_y without and with the singularity subtraction. In Section III, a five-layer generalized anisotropic medium is modeled and compared with the finite element results to verify the algorithm. In addition, the algorithm is applied to the geophysical EM well logging to model triaxial induction logging tools in a five-layer anisotropic medium. Finally, we conclude on the method of EM fields computation in multilayered generalized anisotropic media in Section IV.

II. Electromagnetic Waves in a Homogeneous Anisotropic Medium

A. First-Order Vector Equation

Maxwell's equations in an anisotropic medium can be written as follows:

$$\nabla \times \mathbf{H}(\mathbf{r}) = j\omega\bar{\bar{\epsilon}}\mathbf{E}(\mathbf{r}) + \mathbf{J} \tag{1}$$

$$\nabla \times \mathbf{E}(\mathbf{r}) = -j\omega\bar{\bar{\mu}}\mathbf{H}(\mathbf{r}) - \mathbf{M} \tag{2}$$

Manuscript received December 28, 2017; revised February 28, 2018; accepted March 24, 2018. *(Corresponding author: Qing Huo Liu.)*

Y. Hu, Y. Fang, D. Wang, and Q. H. Liu are with the Department of Electrical and Computer Engineering, Duke University, Durham, NC 27708 USA (e-mail: yunyun.hu@duke.edu; yuan.fang@duke.edu; dezhi.wang@duke.edu; qhliu@duke.edu).

Y. Zhong is with the Department of Electrical and Computer Engineering, National University of Singapore, Singapore 117576 (e-mail: elezhong@nus.edu.sg).

Color versions of one or more of the figures in this paper are available online at http://ieeexplore.ieee.org.

Digital Object Identifier 10.1109/TGRS.2018.2825430

where $\mathbf{J}$ and $\mathbf{M}$ are arbitrarily oriented electric and magnetic dipole sources, respectively

$$\mathbf{J} = \mathbf{P_e}\delta(x-x')\delta(y-y')\delta(z-z') = \mathbf{P_e}\delta(\mathbf{r}-\mathbf{r}') \tag{3}$$

and

$$\mathbf{M} = \mathbf{P_m}\delta(x-x')\delta(y-y')\delta(z-z') = \mathbf{P_m}\delta(\mathbf{r}-\mathbf{r}'). \tag{4}$$

In Cartesian coordinate system, the tensor $\bar{\bar{\epsilon}}$ and $\bar{\bar{\mu}}$ can be expressed in the form

$$\bar{\bar{\epsilon}} = \begin{pmatrix} \tilde{\epsilon}_{xx} & \tilde{\epsilon}_{xy} & \tilde{\epsilon}_{xz} \\ \tilde{\epsilon}_{yx} & \tilde{\epsilon}_{yy} & \tilde{\epsilon}_{yz} \\ \tilde{\epsilon}_{zx} & \tilde{\epsilon}_{zy} & \tilde{\epsilon}_{zz} \end{pmatrix}, \quad \bar{\bar{\mu}} = \begin{pmatrix} \tilde{\mu}_{xx} & \tilde{\mu}_{xy} & \tilde{\mu}_{xz} \\ \tilde{\mu}_{yx} & \tilde{\mu}_{yy} & \tilde{\mu}_{yz} \\ \tilde{\mu}_{zx} & \tilde{\mu}_{zy} & \tilde{\mu}_{zz} \end{pmatrix}. \tag{5}$$

The complex permittivity and permeability tensors are defined as

$$\bar{\bar{\epsilon}} = \epsilon_0\bar{\bar{\epsilon}}_r - j\frac{\bar{\bar{\sigma}}}{\omega} \tag{6}$$

and

$$\bar{\bar{\mu}} = \mu_0\bar{\bar{\mu}}_r - j\frac{\bar{\bar{\sigma}}_m}{\omega} \tag{7}$$

where $\bar{\bar{\sigma}}$ and $\bar{\bar{\epsilon}}_r$ are the electric conductivity and relative permittivity tensors, respectively, and $\bar{\bar{\sigma}}_m$ and $\bar{\bar{\mu}}_r$ are the magnetic conductivity and relative permeability tensors, respectively. Both $\bar{\bar{\epsilon}}$ and $\bar{\bar{\mu}}$ are complex 3×3 tensors, and can have arbitrary anisotropy.

Performing the following Fourier transforms on Maxwell's equations, one obtains:

$$\mathbf{E}(\mathbf{r}) = \int_{-\infty}^{\infty} dk_x \int_{-\infty}^{\infty} dk_y \tilde{\mathbf{E}}(\mathbf{k_s}, z)\exp(-j\mathbf{k_s}\cdot\boldsymbol{\rho}) \tag{8}$$

and

$$\mathbf{H}(\mathbf{r}) = \int_{-\infty}^{\infty} dk_x \int_{-\infty}^{\infty} dk_y \tilde{\mathbf{H}}(\mathbf{k_s}, z)\exp(-j\mathbf{k_s}\cdot\boldsymbol{\rho}) \tag{9}$$

where $\tilde{\mathbf{E}}$ and $\tilde{\mathbf{H}}$ are electric and magnetic fields in spectral domain, respectively, $\mathbf{k_s} = k_x\hat{x} + k_y\hat{y}$, $\boldsymbol{\rho} = x\hat{x} + y\hat{y}$, and $\mathbf{r} = x\hat{x} + y\hat{y} + z\hat{z}$.

Using (8) and (9), and defining the auxiliary quantities as

$$\varphi(\mathbf{k_s}, z) = \begin{bmatrix} k_x\tilde{H}_x + k_y\tilde{H}_y \\ k_y\tilde{H}_x - k_x\tilde{H}_y \\ k_x\tilde{E}_x + k_y\tilde{E}_y \\ k_y\tilde{E}_x - k_x\tilde{E}_y \end{bmatrix} \tag{10}$$

where $\tilde{H}_x$, $\tilde{H}_y$, $\tilde{E}_x$, and $\tilde{E}_y$ are transverse components in spectral domain, Maxwell's equations can be written as the first-order differential (in z) equation in any region n

$$\frac{d}{dz}\varphi(\mathbf{k_s}, z) = \bar{\bar{\mathbf{A}}}_n\varphi(\mathbf{k_s}, z) + \mathbf{f}\delta(z-z') \tag{11}$$

where $\bar{\bar{\mathbf{A}}}_n$ is a 4×4 matrix whose elements are functions of the spectral variables k_x, k_y and material parameters in region n [15]. $\mathbf{f}$ is the source term having the following expression:

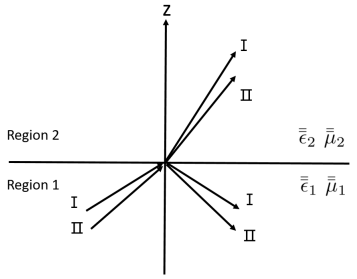

Fig. 1. Incident, reflected, and transmitted waves at the interface of a two-layer anisotropic medium.

$$\mathbf{f} = \begin{pmatrix} k_x & -k_y \\ k_y & k_x \end{pmatrix} \begin{pmatrix} \begin{pmatrix} \tilde{P}_{ey} - \dfrac{\epsilon_{yz}}{\epsilon_{zz}}\tilde{P}_{ez} \\ \tilde{P}_{ex} - \dfrac{\epsilon_{xz}}{\epsilon_{zz}}\tilde{P}_{ez} \end{pmatrix} \\ \begin{pmatrix} -\tilde{P}_{my} + \dfrac{\mu_{yz}}{\mu_{zz}}\tilde{P}_{mz} \\ -\tilde{P}_{mx} + \dfrac{\mu_{xz}}{\mu_{zz}}\tilde{P}_{mz} \end{pmatrix} \end{pmatrix} + \frac{k^2}{\omega} \begin{pmatrix} \dfrac{\tilde{P}_{mz}}{\mu_{zz}} \\ 0 \\ \dfrac{\tilde{P}_{ez}}{\epsilon_{zz}} \\ 0 \end{pmatrix} \tag{12}$$

where

$$\begin{aligned} \tilde{\mathbf{P}_{eq}} &= \frac{1}{4\pi^2}\mathbf{P_e}\hat{q}e^{jk_xx'+jk_yy'} \\ \tilde{\mathbf{P}_{mq}} &= \frac{1}{4\pi^2}\mathbf{P_m}\hat{q}e^{jk_xx'+jk_yy'}, \quad q = x, y, z. \end{aligned} \tag{13}$$

Outside the source region, the general solution to the homogeneous (11) can be written as

$$\begin{aligned} \boldsymbol{\varphi}(\mathbf{k_s}, z) = A_I^+\mathbf{a}_I^+e^{\lambda_I^+z} + A_{II}^+\mathbf{a}_{II}^+e^{\lambda_{II}^+z} + A_I^-\mathbf{a}_I^-e^{\lambda_I^-z} \\ + A_{II}^-\mathbf{a}_{II}^-e^{\lambda_{II}^-z} \end{aligned} \tag{14}$$

where $\mathbf{a}_i$ is the eigenvector corresponding to the ith eigenvalue λ_i. The four eigenvalues represent two types (I and II) of waves going in the positive and negative directions. We define λ_I^+ and λ_{II}^+ for the upgoing waves ($+\hat{z}$), and λ_I^- and λ_{II}^- for the downgoing waves ($-\hat{z}$). Thus, $\varphi(\mathbf{k_s}, z)$ in a homogeneous anisotropic medium becomes

$$\boldsymbol{\varphi}(\mathbf{k_s}, z) = \begin{cases} A_I^+\mathbf{a}_I^+e^{\lambda_I^+z} + A_{II}^+\mathbf{a}_{II}^+e^{\lambda_{II}^+z}, & z > z' \\ A_I^-\mathbf{a}_I^-e^{\lambda_I^-z} + A_{II}^-\mathbf{a}_{II}^-e^{\lambda_{II}^-z}, & z < z'. \end{cases} \tag{15}$$

The coefficients A_I^+, A_{II}^+, A_I^-, and A_{II}^- can be found by integrating the first-order differential equation (11) over the singularity at $z = z'$ with the help of (15). Thus, the EM fields in the homogeneous anisotropic medium can be obtained.

B. Local Transmission and Reflection Matrices

The local transmission and reflection matrices can be obtained by matching boundary conditions in a two-layer anisotropic medium [22], as shown in Fig. 1. For the source in region 1, the field vector in region 1 can be written compactly as

$$\boldsymbol{\varphi}_1(z) = \mathbf{a}_1\ e^{\boldsymbol{\lambda}_1(z-z_1)}\mathbf{A}_1 \tag{16}$$

where $\mathbf{A}_1$ represents the amplitudes of the waves in region 1, $\mathbf{A}_1 = \begin{bmatrix} \mathbf{A}_1^+ \\ \mathbf{A}_1^- \end{bmatrix}$. $\mathbf{A}_1^+$ and $\mathbf{A}_1^-$ represent the wave amplitudes of the upgoing and downgoing waves, respectively. $\boldsymbol{\lambda}_1$ is the diagonal matrix whose ith diagonal element corresponds to the ith eigenvalue, $\boldsymbol{\lambda}_1 = \begin{bmatrix} \boldsymbol{\lambda}_1^+ & \mathbf{0} \\ \mathbf{0} & \boldsymbol{\lambda}_1^- \end{bmatrix}$. We define $\boldsymbol{\lambda}_1^+ = \begin{bmatrix} \lambda_I^+ & 0 \\ 0 & \lambda_{II}^+ \end{bmatrix}$ for two types of upgoing waves and $\boldsymbol{\lambda}_1^- = \begin{bmatrix} \lambda_I^- & 0 \\ 0 & \lambda_{II}^- \end{bmatrix}$ for two types of downgoing waves.

$\mathbf{R}_{12}$ is defined that relates the upgoing waves $(+\hat{z})$ to the downgoing waves $(-\hat{z})$

$$\mathbf{A}_1^- = \mathbf{R}_{12}\mathbf{A}_1^+ \tag{17}$$

where $\mathbf{R}_{12}$ is the reflection matrix from region 2 to 1. With (17), (16) can be written as

$$\boldsymbol{\varphi}_1(z) = \mathbf{a}_1\ e^{\lambda_1(z-z_1)} \begin{bmatrix} \mathbf{I} \\ \mathbf{R}_{12} \end{bmatrix} \mathbf{A}_1^+. \tag{18}$$

In region 2, since only upgoing waves that are the consequence of the transmission of the upgoing waves from region 1 exist, the field vector can be written as

$$\boldsymbol{\varphi}_2(z) = \mathbf{a}_2\ e^{\boldsymbol{\lambda}_2(z-z_1)} \begin{bmatrix} \mathbf{T}_{12} \\ \mathbf{0} \end{bmatrix} \mathbf{A}_1^+ \tag{19}$$

where $\mathbf{T}_{12}$ is the transmission matrix from region 1 to 2; $\boldsymbol{\lambda}_2$ is the eigenvalue diagonal matrix in region 2, and $\boldsymbol{\lambda}_2 = \begin{bmatrix} \boldsymbol{\lambda}_2^+ & \mathbf{0} \\ \mathbf{0} & \boldsymbol{\lambda}_2^- \end{bmatrix}$. Since $\boldsymbol{\varphi}_1(z)$ and $\boldsymbol{\varphi}_2(z)$ are related to the transverse components of the electric and magnetic fields, the boundary conditions require $\boldsymbol{\varphi}_1(z_1) = \boldsymbol{\varphi}_2(z_1)$ at the interface $z = z_1$, leading to

$$\mathbf{a}_1 \begin{bmatrix} \mathbf{I} \\ \mathbf{R}_{12} \end{bmatrix} = \mathbf{a}_2 \begin{bmatrix} \mathbf{T}_{12} \\ \mathbf{0} \end{bmatrix}. \tag{20}$$

The two matrices $\mathbf{R}_{12}$ and $\mathbf{T}_{12}$ can be solved from (20), as $\mathbf{T}_{12} = \hat{a}_{11}^{-1}$ and $\mathbf{R}_{12} = \hat{a}_{21}\mathbf{T}_{12}$, where $\hat{a} = \mathbf{a}_1^{-1}\mathbf{a}_2$.

Similarly, the reflection matrix $\mathbf{R}_{21}$ and transmission matrix $\mathbf{T}_{21}$ can be obtained by assuming the source in region 2. In region 1, since only the downgoing waves exist, which are the consequence of the transmission of downgoing waves from region 2, the field vector in region 1 can be expressed as

$$\boldsymbol{\varphi}_1(z) = \mathbf{a}_1\ e^{\lambda_1(z-z_1)} \begin{bmatrix} \mathbf{0} \\ \mathbf{T}_{21} \end{bmatrix} \mathbf{A}_2^- \tag{21}$$

where $\mathbf{T}_{21}$ is the transmission matrix from regions 2 to 1. In region 2, the upgoing waves are from the reflection of the downgoing waves

$$\mathbf{A}_2^+ = \mathbf{R}_{21}\mathbf{A}_2^- \tag{22}$$

where $\mathbf{R}_{21}$ is the reflection matrix from region 1 to 2. Therefore, the field vector can be written as

$$\boldsymbol{\varphi}_2(z) = \mathbf{a}_2\ e^{\lambda_2(z-z_1)} \begin{bmatrix} \mathbf{R}_{21} \\ \mathbf{I} \end{bmatrix} \mathbf{A}_2^-. \tag{23}$$

Using the boundary condition at the interface $z = z_1$, we can obtain

$$\mathbf{a}_1 \begin{bmatrix} \mathbf{0} \\ \mathbf{T}_{21} \end{bmatrix} = \mathbf{a}_2 \begin{bmatrix} \mathbf{R}_{21} \\ \mathbf{I} \end{bmatrix}. \tag{24}$$

The two matrices can be solved with (24), as $\mathbf{R}_{21} = -\hat{a}_{11}^{-1}\hat{a}_{12}$ and $\mathbf{T}_{21} = \hat{a}_{22} + \hat{a}_{21}\mathbf{R}_{21}$, where $\hat{a} = \mathbf{a}_1^{-1}\mathbf{a}_2$. Thus, the fields in a half-space anisotropic medium can be computed.

C. Global Reflection Matrices and Wave Amplitudes

For multilayered anisotropic media, the proposed method relies on the downward and upward-going recursion relations which transfer the transverse EM fields from one interface to the next in accordance with the boundary conditions. This procedure ensures all the fields information at one interface is effectively passed on to the next. The global reflection matrices and the recursion relations of the wave amplitudes at each interface are derived as follows.

Assuming z' in the mth region, the field vector in region i $(i > m)$ can be written as

$$\boldsymbol{\varphi}_i(z) = \mathbf{a}_i^+ e^{\boldsymbol{\lambda}_i^+(z-z_i)}\mathbf{A}_i^+ + \mathbf{a}_i^- e^{\boldsymbol{\lambda}_i^-(z-z_i)}\mathbf{A}_i^- \tag{25}$$

where $\boldsymbol{\lambda}_i^+$ and $\boldsymbol{\lambda}_i^-$ are the eigenvalue vectors of the upgoing and downgoing waves, respectively; $\mathbf{a}_i^+$ and $\mathbf{a}_i^-$ are the corresponding eigenvectors; and $\mathbf{A}_i^+$ and $\mathbf{A}_i^-$ are the amplitudes of the upgoing and downgoing waves defined at the interface z_i.

For the fields in the $(i+1)$th region, the field vector can be written as

$$\boldsymbol{\varphi}_{i+1}(z) = \mathbf{a}_{i+1}^+ e^{\boldsymbol{\lambda}_{i+1}^+(z-z_{i+1})}\mathbf{A}_{i+1}^+ + \mathbf{a}_{i+1}^- e^{\boldsymbol{\lambda}_{i+1}^-(z-z_{i+1})}\mathbf{A}_{i+1}^-. \tag{26}$$

The global reflection matrices $\tilde{\mathbf{R}}_{i,i+1}$ and $\tilde{\mathbf{R}}_{i+1,i+2}$ are defined to relate the upoing waves to the downgoing waves in regions i and $i+1$, respectively

$$\mathbf{A}_i^- = \tilde{\mathbf{R}}_{i,i+1}\mathbf{A}_i^+ \tag{27}$$

and

$$\mathbf{A}_{i+1}^- = \tilde{\mathbf{R}}_{i+1,i+2}\mathbf{A}_{i+1}^+. \tag{28}$$

At the interface $z = z_i$, the downgoing waves in region i are the consequence of the reflection of the upgoing waves in region i and the transmission of the downgoing waves from region $i+1$, hence

$$\tilde{\mathbf{R}}_{i,i+1}\mathbf{A}_i^+ = \mathbf{R}_{i,i+1}\mathbf{A}_i^+ + \mathbf{T}_{i+1,i}e^{\boldsymbol{\lambda}_{i+1}^-(z_i-z_{i+1})}\tilde{\mathbf{R}}_{i+1,i+2}\mathbf{A}_{i+1}^+ \tag{29}$$

where $\mathbf{R}_{i,i+1}$ is the local reflection matrix from region $i+1$ to i and $\mathbf{T}_{i+1,i}$ is the local transmission matrix from region $i+1$ to i. Similarly, at $z = z_i$, the upgoing waves in region $i+1$ are the consequence of the reflection of the downgoing waves in region $i+1$ and the transmission of the upgoing waves from region i, hence

$$e^{\boldsymbol{\lambda}_{i+1}^+(z_i-z_{i+1})}\mathbf{A}_{i+1}^+ = \mathbf{R}_{i+1,i}e^{\boldsymbol{\lambda}_{i+1}^-(z_i-z_{i+1})}\tilde{\mathbf{R}}_{i+1,i+2}\mathbf{A}_{i+1}^+ + \mathbf{T}_{i,i+1}\mathbf{A}_i^+. \tag{30}$$

From (30), $\mathbf{A}_{i+1}^+$ can be obtained as

$$\mathbf{A}_{i+1}^+ = [e^{\boldsymbol{\lambda}_{i+1}^+(z_i-z_{i+1})} - \mathbf{R}_{i+1,i}e^{\boldsymbol{\lambda}_{i+1}^-(z_i-z_{i+1})}\tilde{\mathbf{R}}_{i+1,i+2}]^{-1} \times \mathbf{T}_{i,i+1}\mathbf{A}_i^+ \tag{31}$$

where $\mathbf{R}_{i+1,i}$ is the local reflection matrix from region i to $i+1$ and $\mathbf{T}_{i,i+1}$ is the local transmission matrix from region i to $i+1$. Equation (31) can be used recursively to obtain the amplitudes in $i > m$ region. Using (31), the global reflection matrix can be obtained from (29)

$$\begin{aligned}\tilde{\mathbf{R}}_{i,i+1} &= \mathbf{R}_{i,i+1} + \mathbf{T}_{i+1,i} e^{\boldsymbol{\lambda}_{i+1}^{-}(z_i - z_{i+1})} \tilde{\mathbf{R}}_{i+1,i+2} \\ &\quad \times \left[e^{\boldsymbol{\lambda}_{i+1}^{+}(z_i - z_{i+1})} - \mathbf{R}_{i+1,i} e^{\boldsymbol{\lambda}_{i+1}^{-}(z_i - z_{i+1})} \right. \\ &\quad \left. \times \tilde{\mathbf{R}}_{i+1,i+2} \right]^{-1} \mathbf{T}_{i,i+1}. \end{aligned} \tag{32}$$

For the fields in region i ($i < m$), the field vector can be written as

$$\boldsymbol{\varphi}_i(z) = \mathbf{a}_i^{+} e^{\boldsymbol{\lambda}_i^{+}(z - z_{i-1})} \mathbf{A}_i^{+} + \mathbf{a}_i^{-} e^{\boldsymbol{\lambda}_i^{-}(z - z_{i-1})} \mathbf{A}_i^{-} \tag{33}$$

where $\mathbf{A}_i^{+}$ and $\mathbf{A}_i^{-}$ are the amplitudes of the upgoing and downgoing waves defined at the interface z_{i-1}. The field vector in the $(i+1)$th region can be written as

$$\boldsymbol{\varphi}_{i+1}(z) = \mathbf{a}_{i+1}^{+} e^{\boldsymbol{\lambda}_{i+1}^{+}(z - z_i)} \mathbf{A}_{i+1}^{+} + \mathbf{a}_{i+1}^{-} e^{\boldsymbol{\lambda}_{i+1}^{-}(z - z_i)} \mathbf{A}_{i+1}^{-}. \tag{34}$$

The global reflection matrices $\tilde{\mathbf{R}}_{i+1,i}$ and $\tilde{\mathbf{R}}_{i,i-1}$ that relate the upoing waves to the downgoing waves in regions i and $i+1$, respectively, are defined as

$$\mathbf{A}_i^{+} = \tilde{\mathbf{R}}_{i,i-1} \mathbf{A}_i^{-} \tag{35}$$

and

$$\mathbf{A}_{i+1}^{+} = \tilde{\mathbf{R}}_{i+1,i} \mathbf{A}_{i+1}^{-}. \tag{36}$$

At the interface $z = z_i$, the downgoing waves in region i are the consequence of the reflection of the upgoing wave in region i and the transmission of the downgoing waves from region $i+1$, hence

$$e^{\boldsymbol{\lambda}_i^{-}(z_i - z_{i-1})} \mathbf{A}_i^{-} = \mathbf{R}_{i,i+1} e^{\boldsymbol{\lambda}_i^{+}(z_i - z_{i-1})} \tilde{\mathbf{R}}_{i,i-1} \mathbf{A}_i^{-} + \mathbf{T}_{i+1,i} \mathbf{A}_{i+1}^{-}. \tag{37}$$

Similarly, at $z = z_i$, the upgoing waves in region $i+1$ are the consequence of the reflection of the downgoing waves in region $i+1$ and the transmission of the upgoing wave from region i, hence

$$\tilde{\mathbf{R}}_{i+1,i} \mathbf{A}_{i+1}^{-} = \mathbf{R}_{i+1,i} \mathbf{A}_{i+1}^{-} + \mathbf{T}_{i,i+1} e^{\boldsymbol{\lambda}_i^{+}(z_i - z_{i-1})} \tilde{\mathbf{R}}_{i,i-1} \mathbf{A}_i^{-}. \tag{38}$$

From (37), $\mathbf{A}_i^{-}$ can be written as

$$\begin{aligned}\mathbf{A}_i^{-} &= [e^{\boldsymbol{\lambda}_i^{-}(z_i - z_{i-1})} - \mathbf{R}_{i,i+1} e^{\boldsymbol{\lambda}_i^{+}(z_i - z_{i-1})} \tilde{\mathbf{R}}_{i,i-1}]^{-1} \\ &\quad \times \mathbf{T}_{i+1,i} \mathbf{A}_{i+1}^{-}. \end{aligned} \tag{39}$$

Equation (39) can be used recursively to find the wave amplitudes in regions $i < m$. The global reflection matrix can be obtained from (38)

$$\begin{aligned}\tilde{\mathbf{R}}_{i+1,i} &= \mathbf{R}_{i+1,i} + \mathbf{T}_{i,i+1} e^{\boldsymbol{\lambda}_i^{+}(z_i - z_{i-1})} \tilde{\mathbf{R}}_{i,i-1} \\ &\quad \times [e^{\boldsymbol{\lambda}_i^{-}(z_i - z_{i-1})} - \mathbf{R}_{i,i+1} e^{\boldsymbol{\lambda}_i^{+}(z_i - z_{i-1})} \tilde{\mathbf{R}}_{i,i-1}]^{-1} \mathbf{T}_{i+1,i}. \end{aligned} \tag{40}$$

For the fields in region m ($i = m$), when $z > z'$, the field vector can be written as

$$\boldsymbol{\varphi}_m(z, z') = \mathbf{a}_m^{+} e^{\boldsymbol{\lambda}_m^{+} z} \left(\mathbf{A}_D^{+} + \mathbf{A}_m^{+} \right) + \mathbf{a}_m^{-} e^{\boldsymbol{\lambda}_m^{-} z} \mathbf{A}_m^{-}. \tag{41}$$

Assuming that

$$\mathbf{A}_D^{+} + \mathbf{A}_m^{+} = e^{-\boldsymbol{\lambda}_m^{+} z_m} \mathbf{A}_m^{+''} \tag{42}$$

and

$$\mathbf{A}_m^{-} = e^{-\boldsymbol{\lambda}_m^{-} z_m} \mathbf{A}_m^{-''}. \tag{43}$$

Equation (41) becomes

$$\boldsymbol{\varphi}_m(z, z') = \mathbf{a}_m^{+} e^{\boldsymbol{\lambda}_m^{+}(z - z_m)} \mathbf{A}_m^{+''} + \mathbf{a}_m^{-} e^{\boldsymbol{\lambda}_m^{-}(z - z_m)} \mathbf{A}_m^{-''}. \tag{44}$$

The upgoing and downgoing waves are related by the global reflection matrix at the interface $z = z_m$

$$\mathbf{A}_m^{-''} = \tilde{\mathbf{R}}_{m,m+1} \mathbf{A}_m^{+''}. \tag{45}$$

From (42), (43), and (45), $\mathbf{A}_m^{-}$ can be obtained as

$$\mathbf{A}_m^{-} = e^{-\boldsymbol{\lambda}_m^{-} z_m} \tilde{\mathbf{R}}_{m,m+1} e^{\boldsymbol{\lambda}_m^{+} z_m} \left(\mathbf{A}_D^{+} + \mathbf{A}_m^{+} \right) \tag{46}$$

where $\mathbf{A}_D^{+}$ represents the amplitudes of the upgoing primary fields.

When $z < z'$, the fields can be expressed as

$$\boldsymbol{\varphi}_m(z, z') = \mathbf{a}_m^{+} e^{\boldsymbol{\lambda}_m^{+} z} \mathbf{A}_m^{+} + \mathbf{a}_m^{-} e^{\boldsymbol{\lambda}_m^{-} z} \left(\mathbf{A}_D^{-} + \mathbf{A}_m^{-} \right) \tag{47}$$

where $\mathbf{A}_D^{-}$ represents the amplitudes of the downgoing primary fields. Assuming that

$$\mathbf{A}_D^{-} + \mathbf{A}_m^{-} = e^{-\boldsymbol{\lambda}_m^{-} z_{m-1}} \mathbf{A}_m^{-'} \tag{48}$$

and

$$\mathbf{A}_m^{+} = e^{-\boldsymbol{\lambda}_m^{+} z_{m-1}} \mathbf{A}_m^{+'}. \tag{49}$$

(47) becomes

$$\boldsymbol{\varphi}_m(z, z') = \mathbf{a}_m^{+} e^{\boldsymbol{\lambda}_m^{+}(z - z_{m-1})} \mathbf{A}_m^{+'} + \mathbf{a}_m^{-} e^{\boldsymbol{\lambda}_m^{-}(z - z_{m-1})} \mathbf{A}_m^{-'}. \tag{50}$$

The upgoing and downgoing waves are related by the global reflection matrix at the interface $z = z_{m-1}$

$$\mathbf{A}_m^{+'} = \tilde{\mathbf{R}}_{m,m-1} \mathbf{A}_m^{-'}. \tag{51}$$

From (48), (49), and (51), $\mathbf{A}_m^{+}$ can be obtained as

$$\mathbf{A}_m^{+} = e^{-\boldsymbol{\lambda}_m^{+} z_{m-1}} \tilde{\mathbf{R}}_{m,m-1} e^{\boldsymbol{\lambda}_m^{-} z_{m-1}} \left(\mathbf{A}_D^{-} + \mathbf{A}_m^{-} \right). \tag{52}$$

By solving (46) and (52), $\mathbf{A}_m^{+}$ can be obtained as

$$\begin{aligned}\mathbf{A}_m^{+} &= \left[\mathbf{I} - e^{-\boldsymbol{\lambda}_m^{+} z_{m-1}} \tilde{\mathbf{R}}_{m,m-1} e^{\boldsymbol{\lambda}_m^{-}(z_{m-1} - z_m)} \tilde{\mathbf{R}}_{m,m+1} e^{\boldsymbol{\lambda}_m^{+} z_m} \right]^{-1} \\ &\quad \times e^{-\boldsymbol{\lambda}_m^{+} z_{m-1}} \tilde{\mathbf{R}}_{m,m-1} e^{\boldsymbol{\lambda}_m^{-} z_{m-1}} \\ &\quad \times \left(\mathbf{A}_D^{-} + e^{-\boldsymbol{\lambda}_m^{-} z_m} \tilde{\mathbf{R}}_{m,m+1} e^{\boldsymbol{\lambda}_m^{+} z_m} \mathbf{A}_D^{+} \right) \Big]. \end{aligned} \tag{53}$$

Using (53), $\mathbf{A}_m^{-}$ can be obtained from (46), and therefore, we obtain the wave amplitudes at the interfaces of the source region. Using the wave amplitudes' relations in (31) and (39) recursively, the wave amplitudes at all other interfaces can

be obtained. In summary, the fields in each region can be computed as

$$\boldsymbol{\varphi}(\mathbf{k_s}, z) = \begin{cases} \mathbf{a}_m e^{\boldsymbol{\lambda}_m (z - z_m)} \begin{pmatrix} \mathbf{I} \\ \tilde{\mathbf{R}}_{m,m+1} \end{pmatrix} \mathbf{A}_m^{+''}, & n = m,\ z > z' \\ \mathbf{a}_m e^{\boldsymbol{\lambda}_m (z - z_{m-1})} \begin{pmatrix} \tilde{\mathbf{R}}_{m,m-1} \\ \mathbf{I} \end{pmatrix} \mathbf{A}_m^{-'}, & n = m,\ z < z' \\ \mathbf{a}_n e^{\boldsymbol{\lambda}_n (z - z_n)} \begin{pmatrix} \mathbf{I} \\ \tilde{\mathbf{R}}_{n,n+1} \end{pmatrix} \mathbf{A}_n^{+}, & n > m \\ \mathbf{a}_n e^{\boldsymbol{\lambda}_n (z - z_{n-1})} \begin{pmatrix} \tilde{\mathbf{R}}_{n,n-1} \\ \mathbf{I} \end{pmatrix} \mathbf{A}_n^{-}, & n < m. \end{cases} \tag{54}$$

D. Singularity Subtraction

For the field location z close to the dipole source location z', the singular nature of the fields needs to be considered [16]. In this paper, the singularity problem is handled by subtracting the primary fields from the background in the spectral domain, and adding the subtracted term in the spatial domain afterward [5]. The singularity subtraction is used to make the integrands' decaying faster. Note that the integration path deforming has already been applied to avoid the singularities along the integration path. The subtraction procedure is shown as follows. Take the $\mathbf{E}$ fields for example

$$\mathbf{E}(\mathbf{r}) = \int_{-\infty}^{\infty} dk_y \int_{-\infty}^{\infty} dk_x [\tilde{\mathbf{E}}(\mathbf{k_s}, z) - \tilde{\mathbf{E}}^{\text{sub}}(\mathbf{k_s}, z)] \times \exp(-j\mathbf{k_s} \cdot \boldsymbol{\rho}) + \mathbf{E}^{\text{add}}(z) \tag{55}$$

where $\mathbf{E}^{\text{add}}(z)$ is the added spatial domain primary fields from the background, and $\tilde{\boldsymbol{E}}^{\text{sub}}(\boldsymbol{k}, z)$ is the corresponding primary fields in the spectral domain. Equation (55) can be rewritten to integrate from 0 to ∞ as follows:

$$\mathbf{E}(\mathbf{r}) = \int_{0}^{\infty} dk_y \int_{0}^{\infty} dk_x [\tilde{\mathbf{e}}(\mathbf{k_s}, z) - \tilde{\mathbf{e}}^{\text{sub}}(\mathbf{k_s}, z)] \times \exp(-j\mathbf{k_s} \cdot \boldsymbol{\rho}) + \mathbf{E}^{\text{add}}(z). \tag{56}$$

The 2-D integration can be calculated in two steps as

$$\tilde{\mathbf{e}}_x(k_y, z) = \int_{0}^{\infty} dk_x [\tilde{\mathbf{e}}(\mathbf{k_s}, z) - \tilde{\boldsymbol{e}}^{\text{sub}}(\mathbf{k_s}, z)] \exp(-j\mathbf{k_s} \cdot \boldsymbol{\rho}) \tag{57}$$

$$\mathbf{E}(\mathbf{r}) = \int_{0}^{\infty} dk_y \tilde{\mathbf{e}}_x(k_y, z) \exp(-jk_y y) + \mathbf{E}^{\text{add}}(z). \tag{58}$$

In the calculation, the upper limit of the integration $k_{x_{max}}$ is determined by adding the segment Δk_x until the desired accuracy is obtained for the first k_y section $[0,\ \Delta k_y]$, and then $k_{x_{max}}$ is fixed in the following k_y integration, as shown in Fig. 2. The primary fields $\boldsymbol{E}^{\text{add}}(z)$ can be calculated by rotating the coordinates, as shown in Fig. 3. The Z-direction of the rotated coordinates is along the direction from the source to the field point. In the rotated coordinates, dZ equals to the distance between the receiver and source. The fields in the rotated coordinates can be calculated unless the distance is small, e.g., the distance less than 0.01 of the skin depth.

A case study is performed to show the convergence of the integrals with the singularity treatment. The model contains

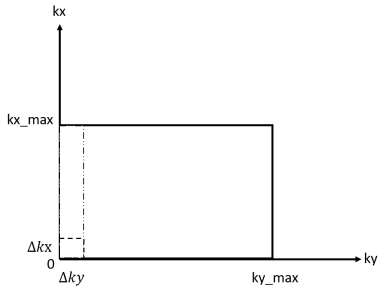

Fig. 2. 2-D integration.

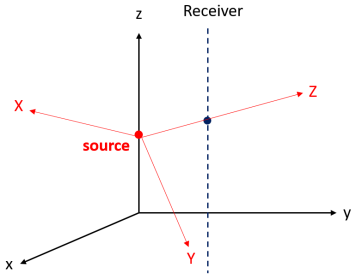

Fig. 3. Coordinate rotation from xyz to XYZ. $\mathbf{Z}$ is along the direction from the source to the receiver.

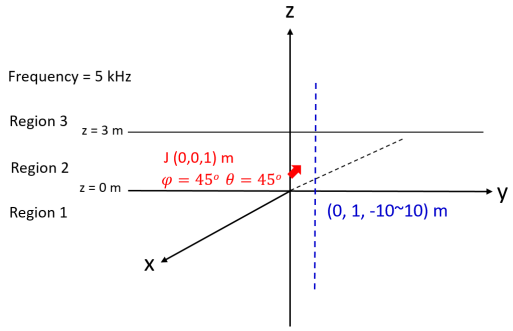

Fig. 4. Three-layer anisotropic medium. The electric dipole source J is oriented at the angle of ($\phi = 45°$, $\theta = 45°$) and located in region 2 (0, 0, 1) m. The receivers align in the z-direction across the three layers at (0, 1, −10:10) m. The frequency is 5 kHz.

TABLE I
THREE-LAYER ANISOTROPIC MEDIUM PROPERTIES

	$\bar{\bar{\mu}}$	$\bar{\bar{\epsilon}}_r$	$\bar{\bar{\sigma}}$
Region 3	$\begin{bmatrix} 7 & 0 & 0 \\ 0 & 5 & 0 \\ 0 & 0 & 8 \end{bmatrix}$	$\begin{bmatrix} 1.0e3 & 0 & 0 \\ 0 & 2.0e2 & 0 \\ 0 & 0 & 5.0e3 \end{bmatrix}$	$\begin{bmatrix} 0.5 & 0 & 0 \\ 0 & 0.9 & 0 \\ 0 & 0 & 1.0 \end{bmatrix}$
Region 2	$\begin{bmatrix} 5 & 0 & 0 \\ 0 & 6 & 0 \\ 0 & 0 & 8 \end{bmatrix}$	$\begin{bmatrix} 5.0e2 & 0 & 0 \\ 0 & 4.0e2 & 0 \\ 0 & 0 & 8.0e2 \end{bmatrix}$	$\begin{bmatrix} 0.6 & 0 & 0 \\ 0 & 0.8 & 0 \\ 0 & 0 & 1.0 \end{bmatrix}$
Region 1	$\begin{bmatrix} 5 & & 0 \\ 0 & 8 & 0 \\ 0 & 0 & 7 \end{bmatrix}$	$\begin{bmatrix} 6.0e2 & 0 & \\ 0 & 4.0e2 & 0 \\ 0 & 0 & 7.0e2 \end{bmatrix}$	$\begin{bmatrix} 0.9 & 0 & 0 \\ 0 & 1.5 & 0 \\ 0 & 0 & 1.0 \end{bmatrix}$

three anisotropic layers. The details of the source and receivers are shown in Fig. 4. The magnetic and dielectric properties of the medium are given in Table I. The high permittivity is primarily due to the double-layer effect as shown in [23]. The EM fields at the receivers are computed and compared with the results of the commercial software Comsol with the

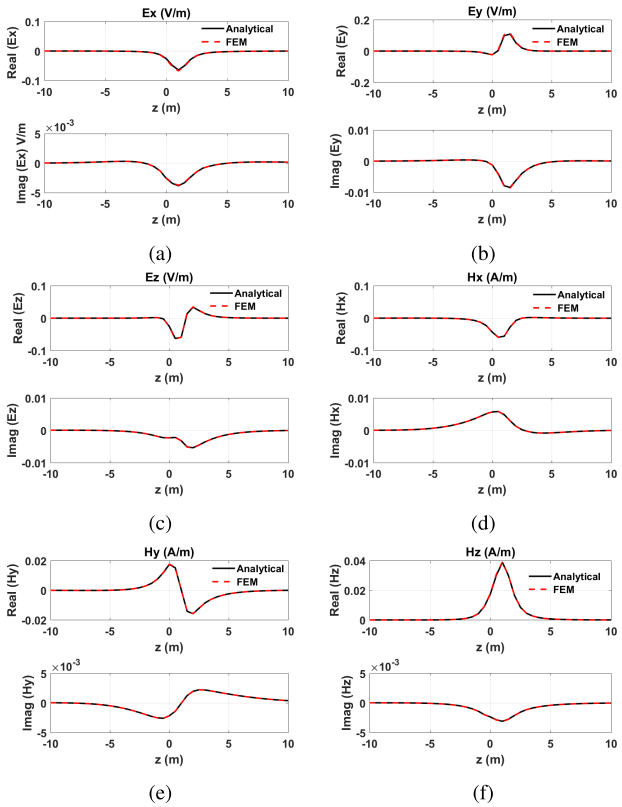

Fig. 5. Comparison with FEM results in the three-layer anisotropic medium with receivers at (0, 1, −10:10) m. (a) E_x. (b) E_y. (c) E_z. (d) H_x. (e) H_y. (f) H_z.

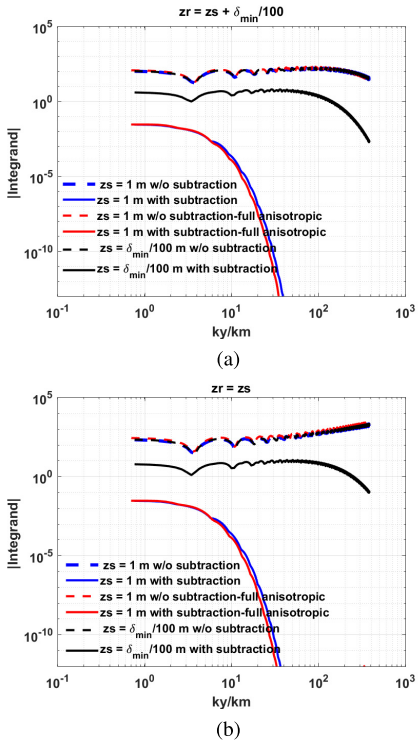

Fig. 6. Comparison between the results with subtraction and without subtraction. (a) $z_r = z_s + \delta_{\min}/100$ m. (b) $z_r = z_s$.

finite element method (FEM) to verify the algorithm. Fig. 5 compares the six components of the EM fields at the receivers, and the two results agree well with each other.

To show the convergence of the integral with subtraction, the magnitude of the integrand with respect to k_y in (58) is calculated.

Three scenarios are modeled and compared. For the first scenario, the source locates in region 2 which is away from the interfaces, as shown in Fig. 4. For the second, the material property tensors are rotated to be full tensors. The z-axis of the tensors is rotated to the angles of ($\phi = 30°$, $\theta = 60°$), while the other conditions remain the same as the first scenario. For the third, the source locates close to the interface ($z = 0$ m) at $z_s = \delta_{\min}/100$ m, while the other conditions remain the same as the first scenario, where $\delta_{\min}$ is defined as the minimum value of the skin depth matrix in the source region.

Fig. 6(a) shows the magnitudes of the integrands with respect to k_y/k_m when z_r is close to the source location z_s ($z_r = z_s + \delta_{\min}/100$), where k_m is defined as $|\omega(\det(\bar{\bar{\epsilon}}\bar{\bar{\mu}})^{(1/3)})^{1/2}|$. It compares the three scenarios with their corresponding integrands without subtraction. As can be seen from the figure, the integrands with subtraction decay rapidly to small values when the source locates away from the interfaces, both for the diagonal and full anisotropic media, while the integrands without subtraction decay much more slowly. When the source locates near the interface, the decaying of the integrands with subtraction becomes much slower. In this case, it will take more steps and needs to integrate over a larger k_y to obtain an accurate solution.

Fig. 6(b) shows the magnitudes of the integrands when $z_r = z_s$, and the other conditions are kept the same. As can be seen from the figure, the integrands with subtraction decrease rapidly when the source locates away from the interfaces, while the integrands without subtraction do not converge. In this case, the fields cannot be calculated without subtraction. When the source locates near the interface, the decaying of the integrands becomes slower even with singularity subtraction.

III. Numerical Results and Discussions

A. Electromagnetic Fields Due to Electric Dipole in a Five-Layer Anisotropic Medium

To verify the algorithm for a multilayered full anisotropic medium, the z-axis of the tensors in Table II is rotated to the angles of $\phi = 60^o$ and $\theta = 30°$ to make them full tensors, as given in Table III. The rotated tensors are used as properties for the five-layer medium. The model and the details of the source and receivers are shown in Fig. 7.

Fig. 8 compares the **E** and **H** fields at the receivers. All components agree well with the FEM results. The good agreement validates the algorithm for multilayered generalized anisotropic media.

B. Application in Geophysical Well Logging

In geophysical EM well logging, formation anisotropy happens commonly, for example, in laminated sand shale and

TABLE II

FIVE-LAYER ANISOTROPIC MEDIUM PROPERTIES—DIAGONAL ANISOTROPY

	$\bar{\bar{\mu}}$	$\bar{\bar{\epsilon}}_r$	$\bar{\bar{\sigma}}$
Region 5	$\begin{bmatrix} 7 & 0 & 0 \\ 0 & 5 & 0 \\ 0 & 0 & 8 \end{bmatrix}$	$\begin{bmatrix} 1.0e3 & 0 & 0 \\ 0 & 2.0e2 & 0 \\ 0 & 0 & 5.0e3 \end{bmatrix}$	$\begin{bmatrix} 0.5 & 0 & 0 \\ 0 & 0.9 & 0 \\ 0 & 0 & 1.0 \end{bmatrix}$
Region 4	$\begin{bmatrix} 5 & 0 & 0 \\ 0 & 6 & 0 \\ 0 & 0 & 8 \end{bmatrix}$	$\begin{bmatrix} 5.0e2 & 0 & 0 \\ 0 & 4.0e2 & 0 \\ 0 & 0 & 8.0e2 \end{bmatrix}$	$\begin{bmatrix} 0.6 & 0 & 0 \\ 0 & 0.8 & 0 \\ 0 & 0 & 1.0 \end{bmatrix}$
Region 3	$\begin{bmatrix} 5 & & 0 \\ 0 & 8 & 0 \\ 0 & 0 & 7 \end{bmatrix}$	$\begin{bmatrix} 6.0e2 & 0 & \\ 0 & 4.0e2 & 0 \\ 0 & 0 & 7.0e2 \end{bmatrix}$	$\begin{bmatrix} 0.9 & 0 & 0 \\ 0 & 1.5 & 0 \\ 0 & 0 & 1.0 \end{bmatrix}$
Region 2	$\begin{bmatrix} 3.5 & & 0 \\ 0 & 2.5 & 0 \\ 0 & 0 & 6 \end{bmatrix}$	$\begin{bmatrix} 5.5e3 & 0 & \\ 0 & 1.0e3 & 0 \\ 0 & 0 & 6.5e2 \end{bmatrix}$	$\begin{bmatrix} 0.65 & 0 & 0 \\ 0 & 1.2 & 0 \\ 0 & 0 & 0.95 \end{bmatrix}$
Region 1	$\begin{bmatrix} 6.5 & & 0 \\ 0 & 4.5 & 0 \\ 0 & 0 & 3 \end{bmatrix}$	$\begin{bmatrix} 6.5e3 & 0 & \\ 0 & 2.0e3 & 0 \\ 0 & 0 & 8.5e2 \end{bmatrix}$	$\begin{bmatrix} 0.75 & 0 & 0 \\ 0 & 1.4 & 0 \\ 0 & 0 & 0.85 \end{bmatrix}$

TABLE III

FIVE-LAYER MEDIUM PROPERTIES—FULL ANISOTROPY

	$\bar{\bar{\mu}}$	$\bar{\bar{\epsilon}}_r$	$\bar{\bar{\sigma}}$
Region 5	$\begin{bmatrix} 6.13 & -0.75 & -1.08 \\ -0.75 & 6.5 & -0.43 \\ -1.08 & -0.43 & 7.38 \end{bmatrix}$	$\begin{bmatrix} 1.55e3 & -0.3e3 & -2.0e3 \\ -0.3e3 & 0.8e3 & -0.17e3 \\ -2.0e3 & -0.17e3 & 3.85e3 \end{bmatrix}$	$\begin{bmatrix} 0.85 & 0.15 & -0.087 \\ 0.15 & 0.6 & 0.087 \\ -0.087 & 0.087 & 0.95 \end{bmatrix}$
Region 4	$\begin{bmatrix} 6.31 & 0.38 & -0.97 \\ 0.38 & 5.25 & 0.22 \\ -0.97 & 0.22 & 7.44 \end{bmatrix}$	$\begin{bmatrix} 518 & -37.5 & -162.38 \\ -37.5 & 475 & -21.65 \\ -162.38 & -21.65 & 706.25 \end{bmatrix}$	$\begin{bmatrix} 0.81 & 0.075 & -0.11 \\ 0.075 & 0.65 & 0.043 \\ -0.11 & 0.043 & 0.94 \end{bmatrix}$
Region 3	$\begin{bmatrix} 7.19 & 1.13 & 0.11 \\ 1.13 & 5.75 & 0.65 \\ 0.11 & 0.65 & 7.06 \end{bmatrix}$	$\begin{bmatrix} 512.5 & -75 & -108.25 \\ -75 & 550 & -43.3 \\ -108.25 & -43.3 & 637.5 \end{bmatrix}$	$\begin{bmatrix} 1.26 & 0.23 & 0.15 \\ 0.23 & 1.05 & 0.13 \\ 0.15 & 0.13 & 1.09 \end{bmatrix}$
Region 2	$\begin{bmatrix} 3.56 & -0.38 & -1.41 \\ -0.38 & 3.25 & -0.22 \\ -1.41 & -0.22 & 5.19 \end{bmatrix}$	$\begin{bmatrix} 1.76e3 & -1.69e3 & 0.64e3 \\ -1.69e3 & 4.38e3 & -0.97e3 \\ 0.64e3 & -0.97e3 & 1.02e3 \end{bmatrix}$	$\begin{bmatrix} 1.03 & 0.21 & 0.049 \\ 0.21 & 0.79 & 0.12 \\ 0.049 & 0.12 & 0.98 \end{bmatrix}$
Region 1	$\begin{bmatrix} 4.5 & -0.75 & 0.866 \\ -0.75 & 6.0 & -0.433 \\ 0.866 & -0.433 & 3.5 \end{bmatrix}$	$\begin{bmatrix} 2.56e3 & -1.69e3 & 0.99e3 \\ -1.69e3 & 5.38e3 & -0.97e3 \\ 0.99e3 & -0.97e3 & 1.42e3 \end{bmatrix}$	$\begin{bmatrix} 1.14 & 0.24 & 0.17 \\ 0.24 & 0.91 & 0.14 \\ 0.17 & 0.14 & 0.95 \end{bmatrix}$

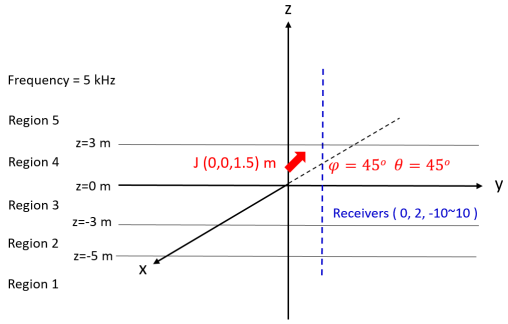

Fig. 7. Five-layer anisotropic medium. The electric dipole source J is oriented at the angle of ($\phi = 45°$, $\theta = 45°$) and located in region 4 (0, 0, 1.5) m. The receivers align in the z-direction across the five layers at (0, 2, −10:10) m.

fractured formations. Measuring the formation electrical properties is crucial for accurate formation evaluation. The triaxial induction logging tool is widely used to measure the formation resistivity anisotropy. The fundamental components of the tool are comprised of three colocated orthogonal transmitters and three colocated orthogonal receivers as shown in Fig. 9.

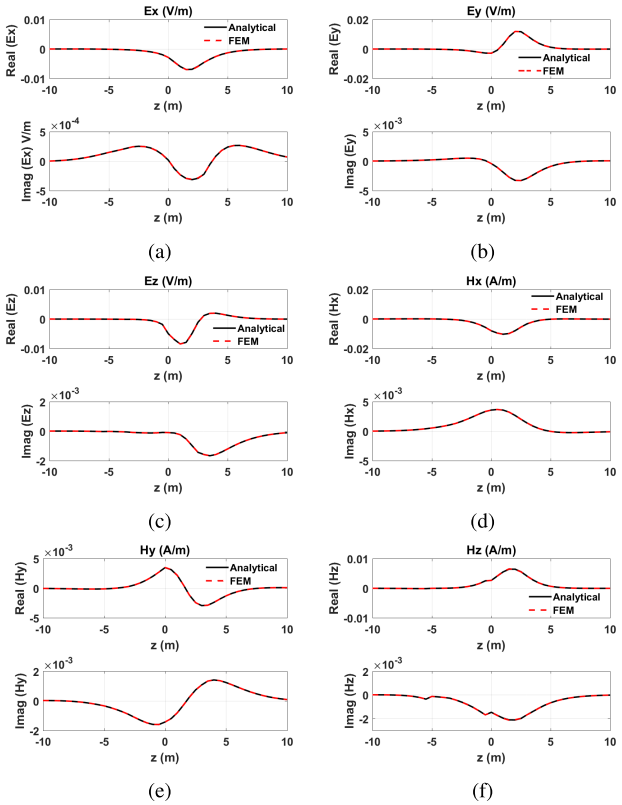

Fig. 8. Fields comparison with FEM results. (a) E_x. (b) E_y. (c) E_z. (d) H_x. (e) H_y. (f) H_z.

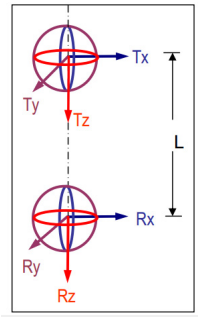

Fig. 9. Basic components of a triaxial induction logging tool. T: transmitter. R: receiver. L: distance between T and R. In this case, the TR spacing is 40 in [24].

Transmitter j couples to receiver i for all $(i, j) = X, Y, Z$, where (X, Y, Z) refers to the tool coordinate system, producing nine coupling components H_i^j of the magnetic fields $\mathbf{H}$

$$\mathbf{H} = \begin{bmatrix} H_X^X & H_Y^X & H_Z^X \\ H_X^Y & H_Y^Y & H_Z^Y \\ H_X^Z & H_Y^Z & H_Z^Z \end{bmatrix}. \tag{59}$$

The measured response is sensitive to the formation anisotropy.

Fig. 10 shows the five-layer anisotropic medium and the triaxial logging tool in two logging trajectories. Transmitters and receivers move together in either a vertical well or deviated well. We compute the $\mathbf{H}$ fields from the T_Z transmitter, resulting in H_X^Z, H_Y^Z, and H_Z^Z components.

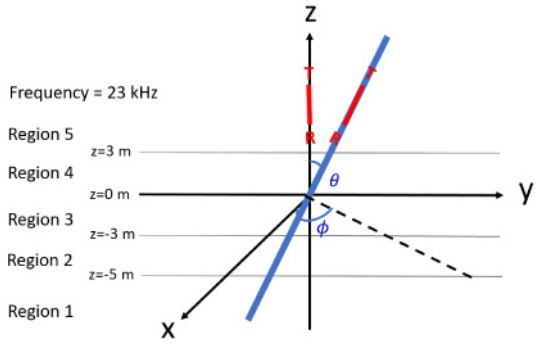

Fig. 10. Triaxial induction tool in a five-layer anisotropic medium. The source is a Z-oriented magnetic dipole T_Z operating at the frequency of 23 kHz. The tool can be in a vertical well or in a deviated well.

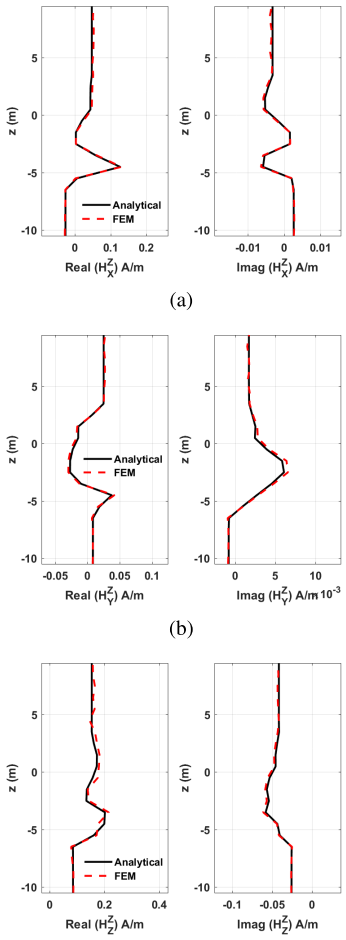

Fig. 11. Triaxial logging response in a vertical well with T_Z. (a) H_X^Z. (b) H_Y^Z. (c) H_Z^Z.

Fig. 11 shows the logging curves in a vertical well and their comparison with the FEM results. Since deviated wells happen commonly in geophysical EM well logging, the logging responses in a deviated well are also modeled and compared with FEM results as shown in Fig. 12. The good agreement further validates the algorithm and shows its capability to model the logging responses in vertical and deviated wells

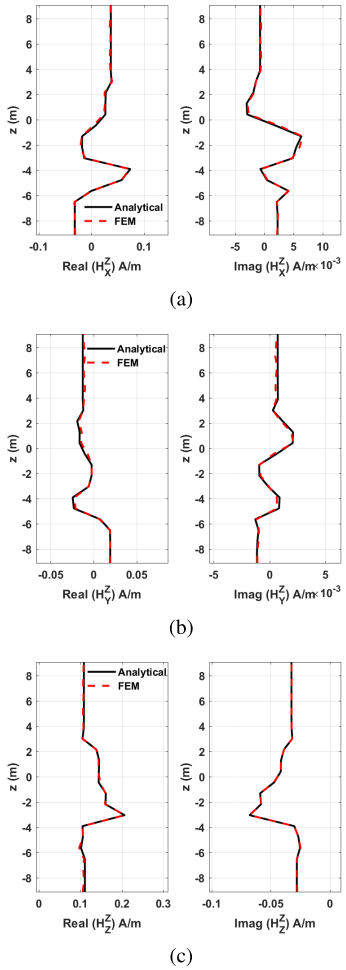

Fig. 12. Triaxial logging response in a deviated well ($\phi = 45°$, $\theta = 30°$) with T_Z. (a) H_X^Z. (b) H_Y^Z. (c) H_Z^Z.

in multilayered anisotropic media. In addition, the anisotropic properties could be conductivity, permittivity, and magnetic permeability or any of their combinations.

IV. Conclusion

In this paper, Maxwell's equations in the spectral domain are formulated into a first-order vector equation concerning the four transverse electric and magnetic field components in a multilayered generalized anisotropic medium. The global reflection matrices and recursion relations of wave amplitudes at interfaces are derived and used to express the four-component vector in any regions. With the Fourier transformation technique, the EM fields in the spatial domain are computed everywhere. The algorithm is capable of modeling both the dielectric and magnetic anisotropy, and both the electric and magnetic sources located in arbitrary regions.

The singular behavior of the fields within the vicinity of the dipole source is treated by subtracting the spectral domain primary fields from the background. A three-layer anisotropic medium is modeled to show the convergence of the integrands with subtraction. The magnitudes of the integrands with subtraction decay rapidly when the source locates away

from the interfaces, both for the diagonal and full anisotropic medium. When the source locates near the interface, the integrands decaying becomes slower, while without subtraction the integrands do not converge when $z_r = z_s$.

To further validate the algorithm, the EM fields in a five-layer generalized anisotropic medium are modeled and compared with the finite element results. The algorithm is also applied to geophysical EM well logging in oil industry where formation anisotropy happens commonly. The triaxial induction logging responses, both in vertical and deviated wells, are modeled and compared with the finite element results. The good agreement shows the capability of the solver to model the induction logging tool in multilayered generalized anisotropic media.

REFERENCES

[1] J. K. Lee and J. A. Kong, "Active microwave remote sensing of an anisotropic random medium layer," *IEEE Trans. Geosci. Remote Sens.*, vol. GE-23, no. 6, pp. 910–923, Nov. 1985.

[2] L.-W. Li, J.-H. Koh, T.-S. Yeo, M.-S. Leong, and P.-S. Kooi, "Cylindrical vector eigenfunction expansion of Green dyadics for multilayered anisotropic media and its application to four-layered forest," *IEEE Trans. Antennas Propag.*, vol. 52, no. 2, pp. 466–477, Feb. 2004.

[3] G. W. Hanson, "Dyadic Green's functions for an anisotropic, non-local model of biased graphene," *IEEE Trans. Antennas Propag.*, vol. 56, no. 13, pp. 747–757, Mar. 2008.

[4] T. V. B. Giang and A. Dreher, "Analysis method of microstrip antennas on hemispherical multilayer structures," *IEEE Trans. Antennas Propag.*, vol. 56, no. 10, pp. 3324–3327, Oct. 2008.

[5] E. Simsek, Q. H. Liu, and B. Wei, "Singularity subtraction for evaluation of Green's functions for multilayered media," *IEEE Trans. Microw. Theory Techn.*, vol. 54, no. 1, pp. 216–225, Jan. 2006.

[6] W. Cai and T. Yu, "Fast calculations of dyadic Green's functions for electromagnetic scattering in a multilayered medium," *J. Comput. Phys.*, vol. 165, no. 1, pp. 1–21, 2000.

[7] J. Wait, "Fields of a horizontal dipole over a stratified anisotropic half-space," *IEEE Trans. Antennas Propag.*, vol. AP-14, no. 6, pp. 790–792, Nov. 1966.

[8] J. A. Kong, "Electromagnetic fields due to dipole antennas over stratified anisotropic media," *Geophysics*, vol. 37, no. 6, pp. 985–996, 1972.

[9] L. Tsang, E. Njoku, and J. A. Kong, "Microwave thermal emission from a stratified medium with nonuniform temperature distribution," *J. Appl. Phys.*, vol. 46, no. 12, pp. 5127–5133, 1975.

[10] S. M. Ali and S. F. Mahmoud, "Electromagnetic fields of buried sources in stratified anisotropic media," *IEEE Trans. Antennas Propag.*, vol. AP-27, no. 5, pp. 671–678, Sep. 1979.

[11] C.-M. Tang, "Electromagnetic fields due to dipole antennas embedded in stratified anisotropic media," *IEEE Trans. Antennas Propag.*, vol. AP-27, no. 5, pp. 665–670, Sep. 1979.

[12] J. K. Lee and J. A. Kong, "Dyadic Green's functions for layered anisotropic medium," *Electromagnetics*, vol. 3, no. 2, pp. 111–130, 1983.

[13] A. Eroglu, Y. H. Lee, and J. K. Lee, "Dyadic Green's functions for multi-layered uniaxially anisotropic media with arbitrarily oriented optic axes," *IET Microw., Antennas Propag.*, vol. 5, no. 15, pp. 1779–1788, Dec. 2011.

[14] C. M. Krowne, "Fourier transformed finding propagation matrix method of characteristics of complex anisotropic layered media," *IEEE Trans. Microw. Theory Techn.*, vol. TMTT-32, no. 12, pp. 1617–1625, Dec. 1984.

[15] J. L. Tsalamengas and N. K. Uzunoglu, "Radiation from a dipole in the proximity of a general anisotropic grounded layer," *IEEE Trans. Antennas Propag.*, vol. AP-33, no. 2, pp. 165–172, Feb. 1985.

[16] J. L. Tsalamengas, "Electromagnetic fields of elementary dipole antennas embedded in stratified general gyrotropic media," *IEEE Trans. Antennas Propag.*, vol. 37, no. 3, pp. 399–403, Mar. 1989.

[17] H.-Y. Yang, "A numerical method of evaluating electromagnetic fields in a generalized anisotropic medium," *IEEE Trans. Microw. Theory Techn.*, vol. 43, no. 7, pp. 1626–1628, Jul. 1995.

[18] H.-Y. D. Yang, "A spectral recursive transformation method for electromagnetic waves in generalized anisotropic layered media," *IEEE Trans. Antennas Propag.*, vol. 45, no. 3, pp. 520–526, Mar. 1997.

[19] Y. Zhong, M. Lambert, D. Lesselier, and X. Chen, "Electromagnetic response of anisotropic laminates to distributed sources," *IEEE Trans. Antennas Propag.*, vol. 62, no. 1, pp. 247–256, Jan. 2014.

[20] E. L. Tan, "Recursive asymptotic impedance matrix method for electromagnetic waves in bianisotropic media," *IEEE Microw. Wireless Compon. Lett.*, vol. 16, no. 6, pp. 351–353, Jun. 2006.

[21] J. Ning and E. L. Tan, "Hybrid matrix method for stable analysis of electromagnetic waves in stratified bianisotropic media," *IEEE Microw. Wireless Compon. Lett.*, vol. 18, no. 10, pp. 653–655, Oct. 2008.

[22] W. C. Chew, *Waves and Fields in Inhomogeneous Media*. Piscataway, NJ, USA: IEEE Press, 1994.

[23] W. C. Chew and P. N. Sen, "Dielectric enhancement due to electrochemical double layer: Thin double layer approximation," *J. Chem. Phys.*, vol. 77, no. 9, pp. 4683–4693, 1982.

[24] H. Wang *et al.*, *Triaxial Induction Logging: Theory, Modeling, Inversion and Interpretation*, document SPE-103897-MS, 2006, pp. 1–19.

Yunyun Hu received the B.S. and M.S. degrees in geophysical well logging from the China University of Petroleum, Qingdao, China, in 2010 and 2013, respectively. She is currently pursuing the Ph.D. degree with the Department of Electrical and Computational Engineering, Duke University, Raleigh, NC, USA.

Her research interests include computational electromagnetics, reservoirs modeling, and subsurface sensing.

Yuan Fang received the B.S. degree in optical engineering from Zhejiang University, Hangzhou, Zhejian, China, in 2013, and the M.S. degree in electrical and computer engineering from Duke University, Durham, NC, USA, in 2016, where he is currently pursuing the Ph.D. degree.

Since 2013, he has been a Research Assistance with the Department of Electrical and Computer Engineering, Duke University. His research interests include computational electromagnetics, inverse algorithms, nanoelectronics, subsurface sensing and imaging, and electromagnetic detection systems.

Dezhi Wang, photograph and biography not available at the time of publication.

Yu Zhong, photograph and biography not available at the time of publication.

Qing Huo Liu (S'88–M'89–SM'94–F'05) photograph and biography not available at the time of publication.